



Full length article

## Structural characterization and viscoelastic constitutive modeling of skin

Vincent R. Sherman<sup>a</sup>, Yizhe Tang<sup>b</sup>, Shiteng Zhao<sup>a</sup>, Wen Yang<sup>a,c</sup>, Marc A. Meyers<sup>a,\*</sup><sup>a</sup> University of California San Diego, La Jolla, CA 92093, USA<sup>b</sup> Shanghai Institute of Applied Mathematics and Mechanics, Shanghai University, Shanghai 200072, People's Republic of China<sup>c</sup> Department of Materials, ETH Zurich, 8093 Zürich, Switzerland

## ARTICLE INFO

## Article history:

Received 22 August 2016

Received in revised form 3 February 2017

Accepted 7 February 2017

Available online 20 February 2017

## Keywords:

Dermis

Collagen

Constitutive equation

Rabbit

Viscosity

## ABSTRACT

A fascinating material, skin has a tensile response which exhibits an extended toe region of minimal stress up to nominal strains that, in some species, exceed 1, followed by significant stiffening until a roughly linear region. The large toe region has been attributed to its unique structure, consisting of a network of curved collagen fibers. Investigation of the structure of rabbit skin reveals that it consists of layers of wavy fibers, each one with a characteristic orientation. Additionally, the existence of two preferred layer orientations is suggested based on the results of small angle X-ray scattering. These observations are used to construct a viscoelastic model consisting of collagen in two orientations, which leads to an in-plane anisotropic response. The structure-based model presented incorporates the elastic straightening and stretching of fibrils, their rotation towards the tensile axis, and the viscous effects which occur in the matrix of the skin due to interfibrillar and interlamellar sliding. The model is shown to effectively capture key features which dictate the mechanical response of skin.

## Statement of Significance

Examination by transmission and scanning electron microscopy of rabbit dermis enabled the identification of the key elements in its structure. The organization of collagen fibrils into flat fibers was identified and incorporated into a constitutive model that reproduces the mechanical response of skin. This enhanced quantitative predictive capability can be used in the design of synthetic skin and skin-like structures.

© 2017 Acta Materialia Inc. Published by Elsevier Ltd. All rights reserved.

## 1. Introduction and background

Skin is an organ of utmost importance, and therefore has been the subject of in-depth research for many years. In 1831, anatomist and surgeon Guillaume Dupuytren observed a patient who claimed to have suffered elliptical stab wounds from a blade with a circular cross-section (a stylet). Due to his disbelief that a circular blade could cause these wounds, Dupuytren experimented on a cadaver and discovered that holes made with a circular knife stretched or closed into ellipses [1]. Karl Langer expanded on this observation and used an ice pick to perforate the skin of cadavers. From these results he proposed lines which exist throughout our body, representing the direction of maximum tension in skin and describing its anisotropy; these are known as Langer lines [2]. Maps of these lines are currently used by surgeons to ensure that incisions heal

quickly and with minimal scarring. Multiple investigations have studied the skin of cat [3], frog [4], rhinoceros [5], and rabbit [6].

Skin is also inspiring modern technology. Replication of certain properties of the skin is highly desirable in many applications such as flexible electronics, soft robotics and prosthetics. The physico-chemical and mechanical design principles of an artificial skin are described by Yannas and Burke [7]; Burke et al. [8] made successful use of a physiologically acceptable artificial skin to treat burn injuries. Today there are a variety of commercial skin substitutes which may be used for therapeutic and testing purposes [9]. Non-biological skins intended for other uses have also been produced; Tee et al. [10] created the first electrically and mechanically self-healing, highly extensible skin for electronics applications by using a composite inorganic nanostructured metal particles in an organic supramolecular polymer host. One interesting constitutive model for the epimysium of muscle, somewhat resembling skin because the collagen is in a wavy configuration, is the one by Gao et al. [11] which assumes a sine shaped collagen fiber integrated with the ground substance.

\* Corresponding author.

E-mail address: [mameyers@ucsd.edu](mailto:mameyers@ucsd.edu) (M.A. Meyers).

The objective of the investigation whose results are presented herein is to provide a mechanistic understanding of the deformation of skin under uniaxial loading. In order to accomplish this, experiments on rabbit skin are compared with a constitutive model based on the straightening of fibers. This model is validated by experiments on idealized circular segments, to which a viscoelastic component is added. This research extends recent work that focused on the tear resistance of skin [6].

## 2. Experimental methods

### 2.1. Natural skin and testing

Butchered and cleaned sexually mature female rabbits were obtained immediately after slaughter from Da Le Ranch in Lake Elsinore, CA. The rabbits were then shaved and skinned. Rabbits were chosen due to a lack of an estrous cycle, which affects the mechanical properties of skin. The use of females reduced variation due to gender differences, so that the effects of varying strain rates may be effectively quantified. Specimens for characterization were frozen in water for preservation. Using surgical blades, skin samples with dimensions of  $20 \times 5 \times 0.6$  mm were cut along directions parallel and perpendicular to the backbone of the rabbit. Uniaxial tensile tests were carried out on an Instron 3342 mechanical testing machine with a load cell of 500N. Preconditioning was not used in order to measure the most natural response of the skin; however, the lack of preconditioning also introduces additional variability in the response. This leads to a more challenging situation with regard to fitting the results, which more closely reflect the natural response of skin. The samples were gripped by the load cell and allowed to hang, at which point the load was tared. Samples were tested with a span of 12 mm at strain rates of  $10^{-1}$  and  $10^{-3} \text{ s}^{-1}$ , and deformation was measured grip-to-grip. These strain rates were chosen so that they would span two orders of magnitude and provide insight into the viscoelastic effects of skin, while remaining within the limitations of our equipment. To retain hydration during tests, phosphate-buffered saline solution was sprayed on the samples periodically.

### 2.2. Scanning and transmission electron microscopy

For SEM observation, undeformed rabbit skin was immersed in 2.5% glutaraldehyde for 3 h to fix the structure, and subsequently dehydrated with an ascending ethanol series. Strips of skin were cut using a surgical blade. Some samples were fractured by freezing in liquid nitrogen. The samples were then dried in a critical point dryer (Tousimis Auto Samdri 815A). The surfaces were sputter coated with iridium using an Emitech K575X and examined using a FEI SFEG ultra-high resolution SEM. For TEM observation, the skin was cut using a scalpel into 5 mm strips. A primary fixation was performed by immersing the tissue sections in 2.5% paraformaldehyde, 2.5% glutaraldehyde in 0.1 M cacodylate buffer for 2 h. Post-fixation was done for 12 h in 1% osmium tetroxide in 0.15 M cacodylate buffer. The specimens were then stained in 1% uranyl acetate for 12 h and dehydrated with an ascending ethanol series, followed by a 1:1 ratio of 100% ethanol and 100% acetone, and finally 100% acetone. Samples were subsequently embedded in Spurr's low-viscosity resin, polymerized at 48 °C for 48 h, and sectioned parallel and normal to the skin surface using a Leica Ultracut UCT ultramicrotome and a Diatome diamond knife. Sections 70–100 nm thick were placed on copper grids for TEM observation, and post stained with Sato lead for 1 min.

### 2.3. Synchrotron X-ray characterization

Uniaxial tensile samples were prepared using a surgical blade and sprayed lightly with phosphate-buffered saline to preserve hydration during testing. These samples were loaded in uniaxial tension at 25 °C, and data was collected throughout the experiment. Biaxial tensile samples were stretched by hand using an embroidery hoop to ~50% biaxial strain, measured optically using a grid drawn on the skin. This is consistent with studies by Lanir and Fung [12], which showed that the heel region of a biaxially stretched sample occurs at stretch ratio of ~1.5. The samples were then fixed in 2.5% glutaraldehyde in order to preserve the stretched structure, followed by dehydration using a graded ethanol series. A surgical blade was used to cut samples for observation from the stretched and fixed skin. All samples were exposed to X-rays at beamline 7.3.3 at the Advanced Light Source synchrotron at the Lawrence Berkeley National Laboratory. A Pilatus2M detector was used to collect data at a distance of ~4 m from the sample.

### 2.4. Simulated tests

A beam of connected circular segments with a circular cross-section was used to model the tensile behavior of a single collagen fibril. The response was verified using a steel beam shaped into circular segments with radius,  $r_c$ , of 30, 60 and 120 mm and angle,  $\omega$ , of 30°, 50°, 70°, 90°, 110° and 130°. The beams were tested in quasistatic tension to verify the model. The geometry is observable in Fig. 5.

### 2.5. Computational techniques

Model geometry was drawn using Solidworks, and imported into COMSOL Multiphysics. One face on the end of the wire was constrained to its initial location, but rotation was allowed. A force was applied to the face on the other end of the wire and pulled along the x axis, while allowing rotation of the face. These conditions avoided errors due to singularities, and resulted in displacements which were converted to strains. Castiglione's theorem was used in the derivation for the straightening of an initially circular segment of a steel wire under tension. Results were plotted in MATLAB.

Root-mean-square error (RMSE) values [13] were calculated between the response predicted by the model and experimental results at strain intervals of 0.01 at  $n$  points, until failure. The resulting value is normalized by the magnitude of stress, resulting in normalized root mean square error (NRMSE):

$$NRMSE = \frac{\sqrt{\sum_{i=1}^n (\sigma_{\text{model}} - \sigma_{\text{experimental}})^2}}{\sigma_{\text{max}} - \sigma_{\text{min}}} \quad (1)$$

## 3. Results and discussion

### 3.1. The hierarchy of the dermis

The dermis is the structural component of skin. It gives the mechanical response required for protection. Collagen (80–90% of dermis) and elastin (3–6%) are the principal proteins responsible for the mechanical properties of the skin [14]. The dermis has been described as an arrangement of wavy fibers, of 2–10 μm in cross-section, which are made of randomly oriented fibrils of ~100 nm in diameter, as shown in Fig. 1a. However, Fig. 1b, which shows intact skin, reveals a well organized structure where the top sur-

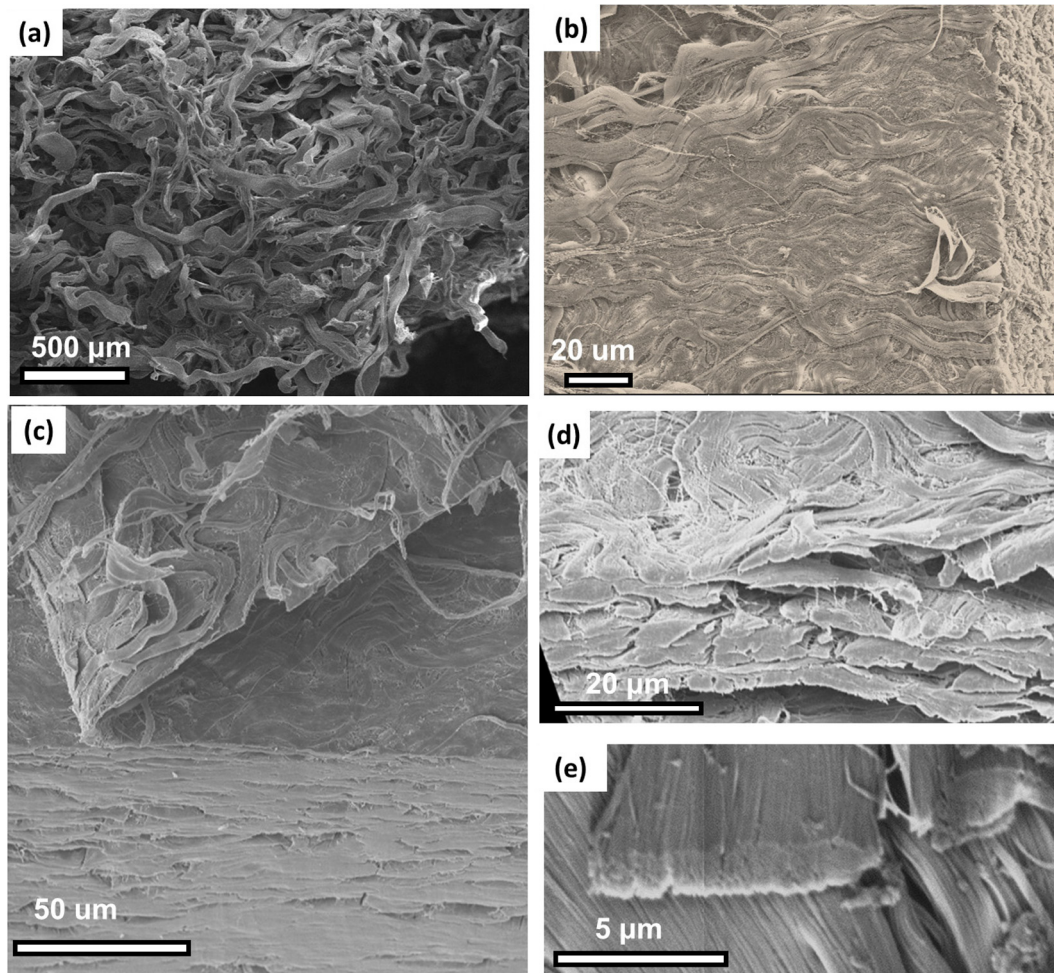


**Fig. 1.** Observation of collagen in rabbit skin by SEM. (a) Fracture surface of skin frozen in liquid nitrogen reveals wavy fibers in apparent disorder. (b) Skin prepared through fixation and peeling: a single layer of collagen fibers is observed in plane with the surface of the skin. (c) One single layer of collagen fibers is peeled from the stack of collagen layers which comprise the thickness of the skin. (d) Several layers of collagen sheets atop each other. (e) Cross-section of single collagen fiber.

face is what appears to be a single layer collagen fibers, aligned in a distinguishable direction. Fig. 1c shows one single layer being peeled from the dermis beneath, illustrating that individual layers have some independence from the layers around them. Fig. 1d shows a skin cross-section, where the layers are observable, and Fig. 1e shows the ends of cut collagen fibers, revealing their shape and cross-sectional dimensions, which are  $\sim 2$  by  $\sim 10$   $\mu\text{m}$ .

The defining small scale features of collagen fibers are more closely observed in Fig. 2 by TEM. Fig. 2a is a TEM of the highly ordered and aligned collagen fibrils within a fiber, in which the characteristic banding present on collagen fibrils is clearly visible. A cut nearly parallel to the skin surface (Fig. 2b) reveals a variety of fibers with fibrils in various orientations, and a cut perpendicular to the surface (Fig. 2c) shows fibers of  $\sim 2$   $\mu\text{m}$  thickness stacked atop each other in the skin.

A full hierarchical description of skin is presented in Fig. 3. Our understanding of the structure incorporates the presence of lamellae with preferred fiber orientations seen in Fig. 1b; adjacent to the renderings of the hierarchical levels are transmission and scanning electron microscopy images of each layer, down to the fibrillar level (Fig. 3b–d).

The smallest spatial scale is well understood for collagen. Fibrils, as seen in Fig. 3b, are approximately 50 nm in diameter and form fibers. However, the organization of fibers into lamellae is less well characterized. We have identified that fibers assemble into

lamellae parallel to the surface of the skin. The approximate cross-sectional dimensions of these ‘flat fibers’ are  $\sim 2$   $\mu\text{m}$  thickness and  $\sim 10$   $\mu\text{m}$  in width. They form a wavy pattern which we model in Section 3.3 as consecutively connected circular segments, but it has also been described as sinusoidal and helical (although it is clear that these fibers are not helical). Fig. 3c shows an SEM image in which multiple fibers are parallel to each other in the skin. These lamellae are arranged in distinct layers where each layer has a specific orientation. In Fig. 3d, a cross-section of the dermis reveals many flat collagen fibers stacked upon each other. For the rabbit skin, the number of fiber/lamella layers is obtained by dividing the dermis thickness (500  $\mu\text{m}$ ) by the thickness of each lamella: (2  $\mu\text{m}$ ); it is approximately 250. Non-collagenous elements, the most prominent of which is elastin, are not shown in Fig. 3 because their relative contributions to the skin’s mechanical properties are less important. Additionally, structural details of the elastin network in skin are currently not well defined.

### 3.2. Deformation imaged by small angle X-ray scattering

Previous studies [6,15] measured the degree of fibril orientation in rabbit skin under uniaxial tension using Small Angle X-ray Scattering (SAXS). Both studies used an orientation index and concluded that the fibrils align with the tensile direction under loading, but information regarding the initial orientation is incon-

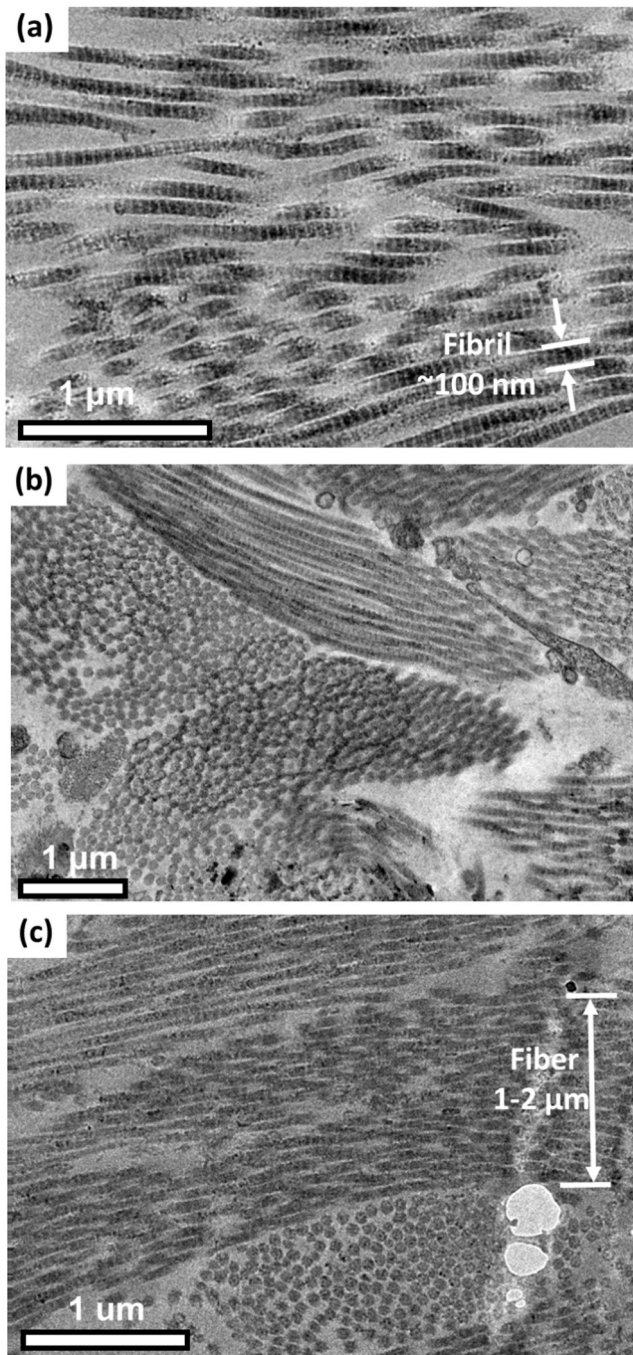


**Fig. 2.** The fibers in skin observed by TEM. (a) TEM shows aligned collagen fibrils in one fiber. (b) TEM cross-section shows multiple collagen fibrils of different orientations. (c) TEM of three collagen fibers stacked vertically.

clusive due to the waviness of the skin which has a high influence on the initially recorded SAXS patterns. Therefore, two deformation paths, shown in Fig. 4, were applied to the skin and analyzed by SAXS: uniaxial and biaxial extension. In uniaxial extension the progression of deformation was characterized along the stress-strain curve at the points marked. Four mechanisms of deformation were found to operate: straightening, rotation (toward the tensile axis), elastic extension of fibers, interfibrillar sliding, and finally fracture [6].

Two positions in the uniaxial extension are marked by open circles on the stress strain curve in Fig. 4a. They correspond to the initial configuration and the one at the maximum load. The original

curved configuration of the collagen fibers and multiple orientations of the lamellae result in an in-plane equiaxed structure, manifested in the SAXS pattern by circular rings which have an intensity that is independent of orientation (Fig. 4b). As uniaxial deformation proceeds there is a gradual alignment of the fibers with the tensile axis. This is shown in Fig. 4c: the SAXS pattern exhibits a higher intensity in the tensile direction (vertical axis).

Biaxial extension straightens the fibers and ideally should enable each lamella to retain its original orientation. Although the progression of biaxial stretching was not monitored, segments of skin subjected to biaxial stretch and then fixed were analyzed. Two representative scattering patterns are shown in Fig. 4d and e. The intensity of the SAXS pattern across the circle corresponds to the fraction of the 250 (estimated) lamellae in this orientation. This radial intensity variation is plotted in Fig. 4f for the four SAXS scans (b, c, d, e). The initial intensity is homogeneous and does not show much variation along the orientations. Uniaxial stretching dramatically changes the pattern and shows the alignment of the collagen fibers with the tensile axis. Interestingly, biaxial stretching introduces some asymmetry in the orientation of the collagen, with an increased intensity in two directions. We attribute this to the preferential alignment of collagen fibers (shown by the analysis and a simplified schematic in Fig. 4g), which is manifested by the Langer lines. Thus, similar to rhinoceros [5] and fish [16] skin, there is some anisotropy in the initial orientations of collagen fibers in the lamellae of rabbit skin.

### 3.3. The constitutive model

The stiffness of collagenous materials is a consequence of the properties, arrangement, and geometric distribution of collagen fibrils. For example, the toe region experienced by many biological materials corresponds to the straightening of the curved arrays of fibrils; when the fibrils are straight the stiffness increases drastically, although it rarely approaches that of the collagen constituents due to the viscous sliding of collagen fibers and fibrils.

The strength of collagenous materials is lower than that of collagen fibrils, which are reported to vary from 200 MPa up to several GPa [17]. Because the strength of skin is well below this, reaching at most  $\sim 50$  MPa (in rhinoceros), failure in tension is the consequence of interfibrillar and interfiber effects, namely the strength and viscoelasticity of bonds between fibrils. The viscoelastic contribution to the failure of skin is readily apparent when observing the fracture strength of rabbit skin measured at differing strain rates: only  $\sim 8$  MPa at a strain rate of  $10^{-3} \text{ s}^{-1}$  compared to  $\sim 15$  MPa at a strain rate of  $10^{-1} \text{ s}^{-1}$  [6]. The model presented is founded on the wavy structure of collagenous materials, but the principal parameters that dictate the response, and principally the intra and interfibrillar shear are expressed through phenomenological parameters leading to a viscosity  $\eta$ .

### 3.4. Elastic component: Derivation

In order to better understand the mechanical response of skin, we model the response of a single collagen fibril. The underlying assumption of this model is that these repeating units dictate the macroscopic material response; by quantitatively characterizing the elastic response of one fibril and the viscous interactions with the matrix we gain an understanding of the mechanical response. Materials consisting of collagen fibrils have been modeled using different shapes including zig zags [18], helices [19,20], and a sine function [21,22]. The limitations of these models were analyzed by Sherman et al. [17], and a circular segment model was suggested as an improved representation of the *in vivo* shape of collagen. Thus, these fibrils are modeled as circular segments, shown in Fig. 5a.

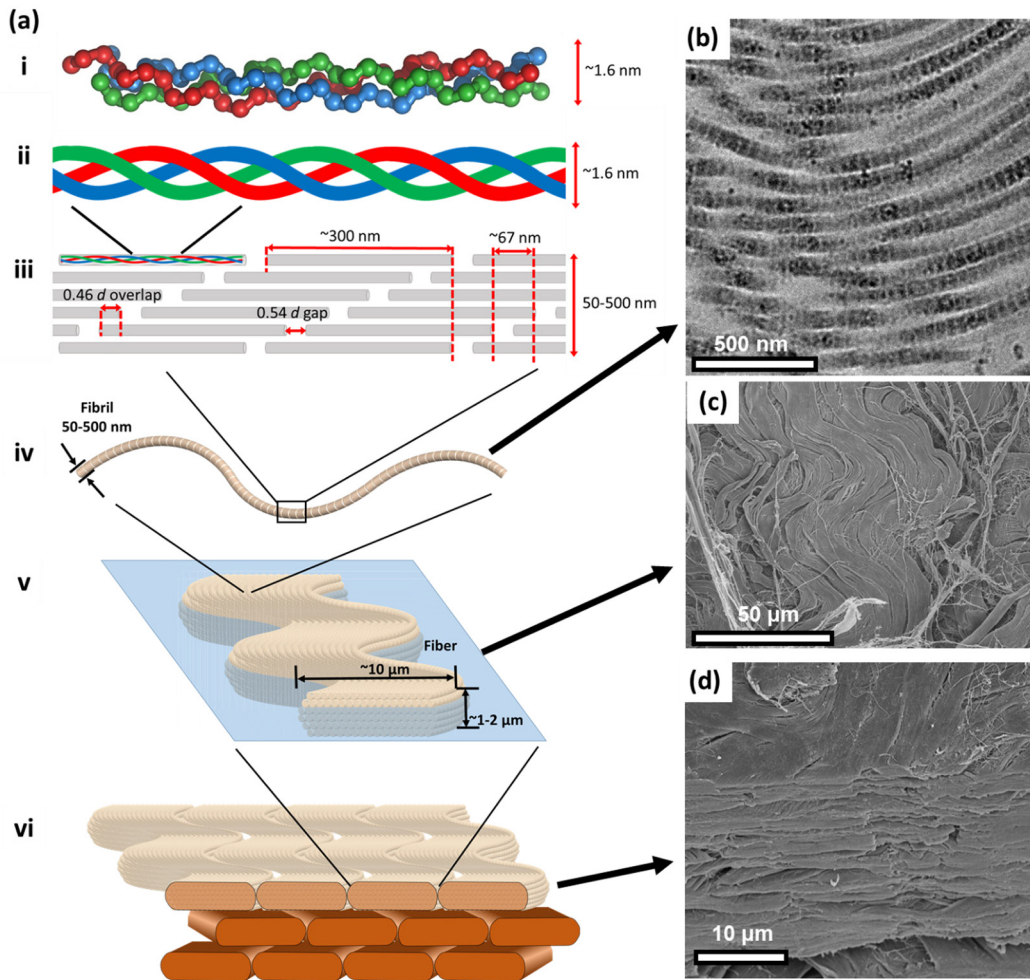


**Fig. 3.** The full hierarchy of collagen in the dermis. (a) Schematic which represents the hierarchy of skin. The hierarchical order is: (i) Tropocollagen chains form right handed triple helices. (ii) Schematic of i. (iii) The fibril is formed through the quarter-staggered arrangement of tropocollagen molecules which leads to a gap region, an overlap region, and characteristic d-banding. (iv) Fibrils are long strands, and the d-banding is clearly evident. (v) Many fibrils are arranged to form wavy parallel fibers, which are flattened in the plane of the skin. (vi) Parallel fibrils form lamellae; these lamellae exist through the thickness of the skin. (b) Transmission electron micrograph of collagen fibrils that are curved and parallel, and form a fiber. (c) Parallel fibers in a single lamella of the skin. (d) Cross-section of skin with multiple lamellae.

In the circular segment model, adjacent segments connect with no discontinuities. Under applied strain, the radius of curvature increases, leading to a decreased segment arc, measured in degrees. One characteristic of these semicircular segments is that there are no discontinuities at their junction, independent of extension. The mechanism of deformation is graphically illustrated in Fig. 5b. Based on the assumed shape and deformation method, the tensile response of a fibril may be calculated using Castigliano's theorem. The problem that must be solved is the following: a curved beam is subjected to a force  $P$  at the ends; determine the load-displacement relationship. The required geometric measurements are schematically described in Fig. 5c and d; Table 1 shows the parameters used in the derivation. In addition to these parameters, relationships between the force, shear force, and bending moment applied to the beam are necessary. These relationships are based on Fig. 5d which shows a cut of the beam.  $Q$  is the shear force acting on the cross-section:

$$Q = P \sin \alpha \quad (2)$$

$N$  is the normal force acting on the cross-section:

$$N = P \cos \alpha \quad (3)$$

and  $M$  is the bending moment:

$$M = -P(y - r_c \sin \theta_0) \quad (4)$$

The strain energy is expressed as the sum of components due to bending, normal force, and shear force, whose equations may be found in Beer et al. [23]. The total strain energy is the sum of the three components of the strain energy obtained from Eqns. S1, S2, and S3 (details provided in Supplementary Materials). From Castigliano's second theorem, the displacement at the point of application of an external force may be expressed as [23]:

$$u = \frac{\partial U}{\partial P} = \frac{\partial U_1}{\partial P} + \frac{\partial U_2}{\partial P} + \frac{\partial U_3}{\partial P} \quad (5)$$

The extension  $u$  in the direction of applied load  $P$  is determined using Eq. (5). Since  $l_0 = r_c \cos \theta_0$ , strain is:

$$\varepsilon = \frac{u}{l_0} = \frac{u}{r_c \cos \theta_0} \quad (6)$$

From the definition of Young's modulus, strain may also be expressed by the ratio of stress/elastic modulus [24]. The modulus is replaced with a pseudo modulus,  $E'$ , as it is not the material modulus,  $E$ , but the result of both structure and material modulus.

$$E' = \frac{P/A}{\varepsilon} = \frac{r_c \cos(\theta_0) P/A}{u} \quad (7)$$

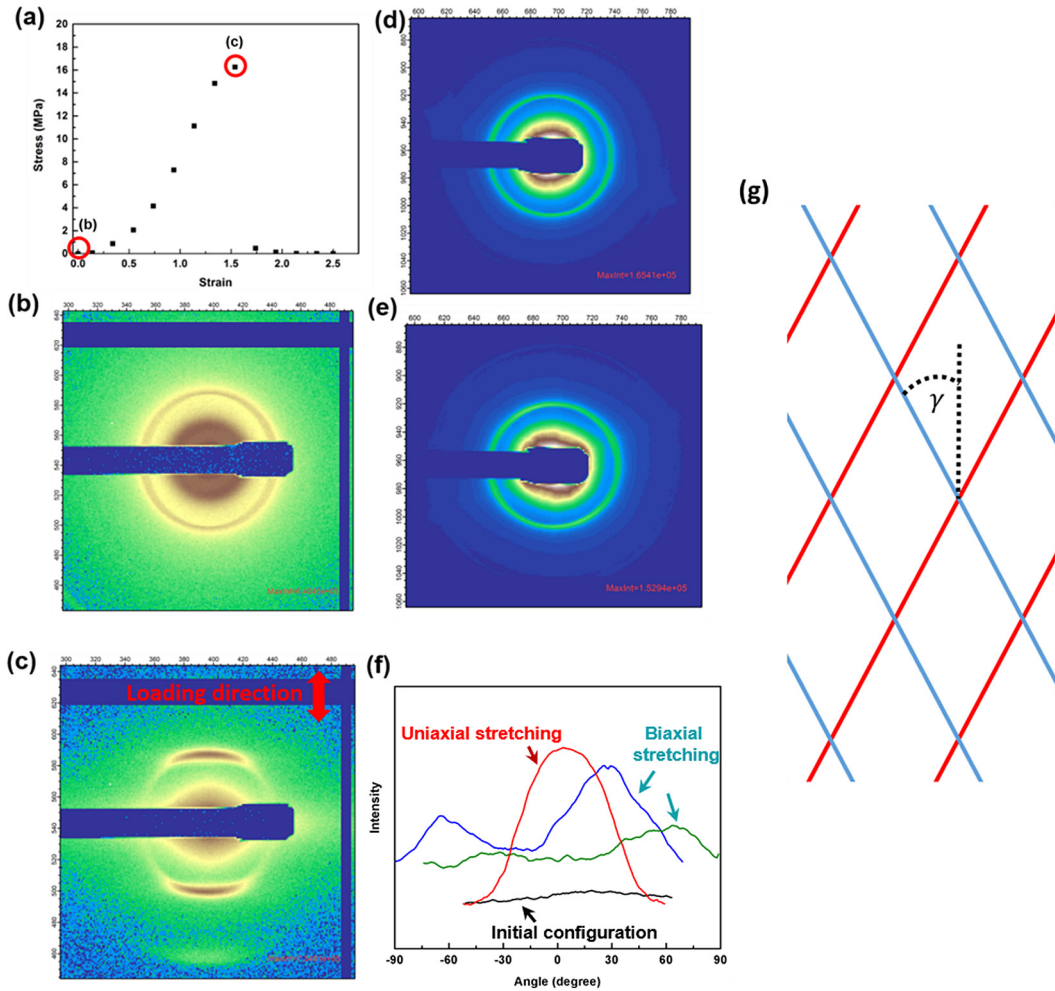


**Fig. 4.** SAXS results show skin has two principal orientations of fibers. (a) Stress-strain curve of the skin; (b) SAXS pattern of the natural skin before uniaxial stretching; (c) SAXS pattern of the skin at the maximum stress (direction of tension shown by arrow); (d, e) SAXS pattern of two fixed skin samples prepared by biaxial stretching; (f) Comparison of SAXS data showing two orientations with increased intensity in biaxially stretched skin, corresponding to two preferred collagen orientations, as seen in rhinoceros [5] and fish [15]. (g) Schematic showing two preferential lamellar directions; these are the two most common of many orientations.

Substituting Eq. (5) into Eq. (7):

$$E' = \frac{r_c \cos(\theta_0) P/A}{\frac{\partial U_1}{\partial P} + \frac{\partial U_2}{\partial P} + \frac{\partial U_3}{\partial P}} \quad (8)$$

Accounting for eccentricity and inserting the results into Eq. (8) leads to a representation of the pseudo modulus in terms of various shape factors, where  $\delta = \frac{H}{r_c}$ ,  $a_y = 1.33$ , and  $E/G = 2(1 + \nu)$ :

$$E' = \frac{E \cos \theta_0}{\phi_2(\theta_0) + \phi_3(\theta_0) \frac{a_y E}{G} + \phi_1(\theta_0) \frac{1}{\left(1 - \frac{\delta^2/4}{2 \left(1 - \sqrt{\left(1 - \frac{\delta}{2}\right) \left(1 + \frac{\delta}{2}\right)}\right)}\right)}} \quad (9)$$

$E'$  is a function of the shape of the circular wire segment. Specifically, the shape parameters required to calculate  $E'$  are thickness ( $H$ ), the initial radius ( $r_c$ ), initial degree of curvature ( $\theta_0 = 90 - \omega_0$ ), and the material modulus  $E$ . Holding arc length constant, the relationship between the strain ( $\varepsilon$ ), current radius ( $r$ ), initial radius ( $r_c$ ), current degree of curvature ( $\omega$ ), and initial degree of curvature ( $\omega_0$ ) is:

$$\varepsilon = \frac{l - l_0}{l_0} = \frac{r \sin\left(\frac{r_c}{r} \omega_0\right) - r_c \sin(\omega_0)}{r_c \sin(\omega_0)} \quad (10)$$

After several additional steps, one arrives at the relationship:

$$\sigma = \int E' \left\{ \frac{\text{CSC } \omega_0}{r_c r} \left[ r \sin\left(\frac{r_c \omega_0}{r}\right) - r_c \phi_0 \cos\left(\frac{r_c \omega_0}{r}\right) \right] \right\} dr \quad (11)$$

Eq. (11) is integrated from  $r_c$  to  $r$  to produce a stress vs strain relationship based on the initial circular shape.

### 3.5. Elastic component: Comparison of experimental, analytical and computed results

In order to validate the model, macroscale tests described in Section 2.4 were performed. By comparing testing results to calculations, we confirm that our model is accurate. The tension setup and stress mapping from a simulation are also shown in Fig. 6a. The results are illustrated in Fig. 6b for three curves with 30 mm radius and  $\omega_0 = 70^\circ$ : one from calculations (solid line), one from tensile tests (dashed line), and one from simulations (dotted line). There is excellent agreement among them. Fig. 6c shows the dramatic effect that varying the curvature can have on the elastic response, as larger values of  $\omega_0$  substantially increase strain achievable at low stresses. Similarly, calculations with a constant degree of curvature but different radii are shown in Fig. 6d, indicating the profound effect that radius (more precisely, ratio of beam thickness to radius) can have on test results. In the biological context of collagen, this indicates the substantial effect that the thick-

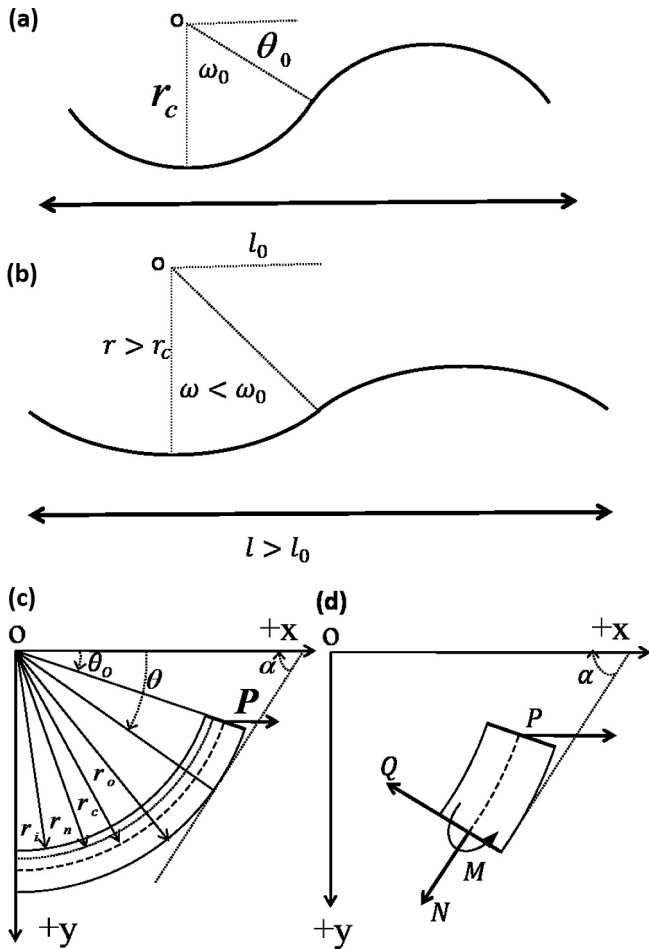


**Fig. 5.** Circular segment model of collagen. (a and b) Behavior of model under extension. Initial curvature  $\omega_0$  decreases to  $\omega$ . Initial radius  $r_c$  increases to  $r$ . Total length increases from  $l_0$  to  $l$ . (c) A section of the circular segment collagen model, showing relevant parameters which are required for the strain energy and corresponding stress calculation using Castiglino's theorem. (d) Free-body diagram of a wire segment showing  $P$  (applied force). The method-of-sections replaces the removed part with  $N$  (normal force),  $Q$  (shearing force), and  $M$  (bending moment).

**Table 1**  
Parameters used in derivation of constitutive equation.

Symbol	Parameter
$\omega_0$	Initial angle of waviness
$\omega$	Current angle of waviness
$r_i$	Inner radius of curvature
$r_o$	Outer radius of curvature
$r_c$	Radius of curvature at the centroidal axis
$r_n$	Initial radius of curvature for the neutral axis
$e$	Eccentricity, $e = r_c - r_n$
$A$	Cross-section area
$H$	Height of the curved beam, $H = r_o - r_i$
$\theta_0$	Description of degree of curvature
$\theta$	Description of location on the semicircular curve

ening of fibrils (often associated with ageing) may have on the mechanical response of collagenous materials.

### 3.6. Elastic component: Application

The complete calculation of the elastic component of stress involves three stages:

- 1) Stress on a straightening circular segment is calculated. Fibril dimensions are applied, as estimated from SEM images. Strain is calculated using Eq. (10), and stress is calculated using Eq. (11).
- 2) The calculated strain from Eq. (10) is divided by the cosine of the estimated average degree of misorientation from the tensile axis ( $\gamma$ ), determined by comparing the onset of the heel region of different orientations. This is based on the biaxial SAXS data which suggests two preferred fibril directions, as shown in Fig. 4f. This step accounts for the ability of fibrils to rotate.

$$\varepsilon = \frac{\varepsilon_{\text{semicircular}}}{\cos(\gamma)} \quad (12)$$

- 3) A maximum stiffness is applied which reflects the physical response of the skin [6], and is a property of collagen fibers in tension:

$$\sigma_{\text{shape,orientation,fiber-stiffness}} = \int \min\left(\frac{d\sigma_{\text{shape,orientation}}}{d\varepsilon}, E_{\text{max}}\right) d\varepsilon \quad (13)$$

This effect may be due to the stretching of the bonds between fibrils and fibers, and the continued recruitment of fibrils. These affect the true strength and stiffness of collagen fibrils, which are not reached in the skin, and leads to the presence of a linear region which is at a substantially decreased stiffness compared to that of a collagen fibril.

### 3.7. Incorporation of viscosity into the elastic model

Uniaxial tests show clear differences from the model which are attributable to the viscosity of skin [6]. The viscous effects of skin dissipate a large amount of energy, and lead to lower failure strengths, due to the larger sliding time. Previous descriptions of the elasticity and viscoelasticity of skin have resulted in a number of constitutive equations and mathematical curve fits. However, no relationship which directly considers the physical shape, viscosity, and orientation effects of skin has been successfully developed, other than the model by Yang et al. [6]; it approximates the tensile response of the skin with circular segments in a Maxwell arrangement, and produces acceptable results for curves with a small toe region. This relationship, representative of a spring and dashpot in series, leads to a large extension with low levels of stress at a sufficiently low strain rate, and decaying stress when strain is no longer applied. However, Shaw and MacKnight [25] suggested that the Maxwell model is a poor representation of viscoelastic bodies such as polymers.

In the case of rabbit skin, a low strain rate leads to reduced maximum stress levels; however, the amount of extension is not largely affected when the strain rate varies by a factor of 100. Therefore, we apply a Kelvin-Voigt model, which is better suited for use in a viscoelastic solid [25]. The spring, shaped as consecutively connected circular segments, is in parallel with a dashpot. As the parallel spring and dashpot experience equivalent strain, the total stress is equal to the sum of the elastic stress and viscous stresses.

The elastic stress is obtained from Eqs. (11) to (13). There are two regimes: straightening of the fibers (Eq. (11)) and their elastic extension; both are incorporated into Eq. (13). For the viscous component, the general form is used (e. g., Meyers and Chawla [26]):

$$\eta = K\dot{\varepsilon}^n \quad (14)$$

Eq. (14) adjusts viscosity based on strain rate;  $n < 0$  is shear thinning,  $n = 0$  is Newtonian viscosity, and  $n > 0$  is shear thickening.

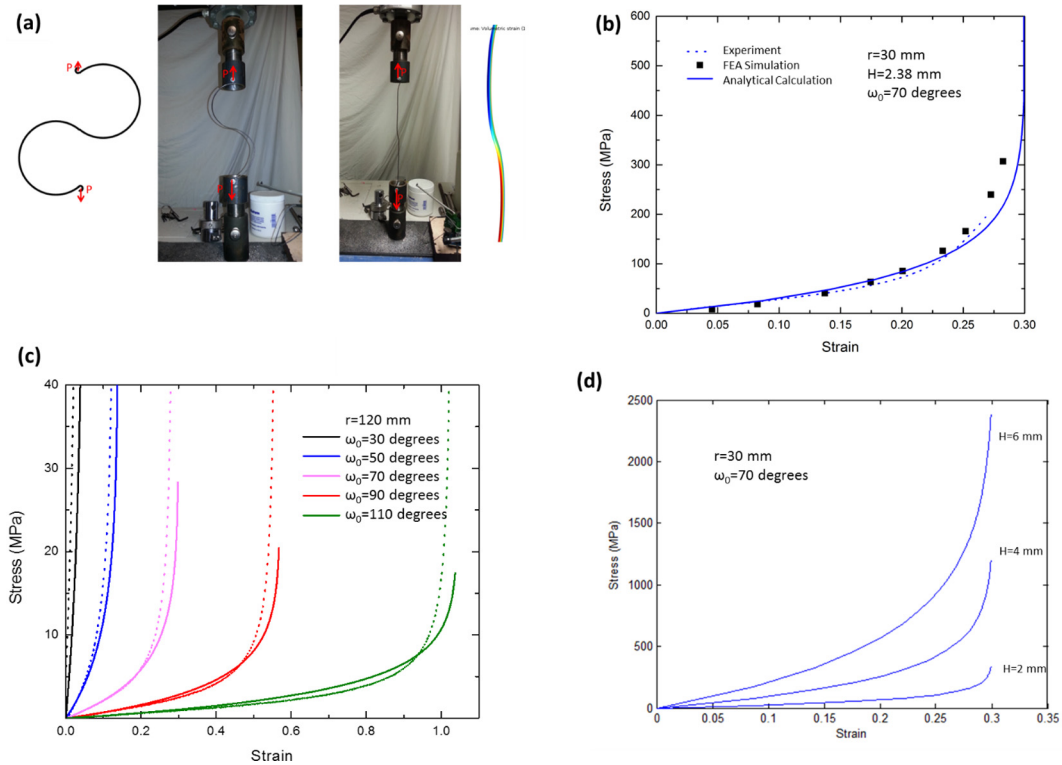


**Fig. 6.** Validation of elastic model. (a) Tests performed by mechanical testing (left) and finite element analysis (right). (b) Comparison of results obtained by testing, calculations, and simulations for  $r = 30$  mm and  $\omega_0 = 60$  show close agreement. (c) Calculation and testing results from various degrees of curvature while holding  $r = 30$  constant show close agreement between calculations and tests, and illustrate the drastic effect that increasing the degree of curvature may have on both stress and strain. (d) Calculation results showing the effects increasing radius for  $\omega_0 = 70^\circ$ . Increasing radius reduces the ratio of beam thickness to radius, which significantly reduces stress values.

Shear thinning is a reduction in viscosity with increasing strain rate. Finlay [27] studied viscosity in human skin, and concluded that viscoelastic models of skin should account for shear thinning phenomenon if the theoretical results were to bear any relation to real life data under both static and dynamic conditions. The viscous stress occurs within the ground substance that connects fibers and fibrils of collagen. During the toe region of the curve, reorientation does not involve viscous effects in a significant manner. In the heel and linear region, the fibers are stretched and the viscous effects become more prominent. Therefore, the viscous component of stress is applied proportionally to the ratio of current strain ( $\varepsilon$ ) to the strain at the onset of the heel, ( $\varepsilon_{heel}$ ), raised to the power of  $\alpha$ ; this is the fibril recruitment fitting parameter. Each viscoelasticity parameter ( $\alpha, K, n$ ) has a unique effect on the response. The parameter  $\alpha$  affects the rate at which viscosity is applied to fiber recruitment; a value of 1 means that the fiber recruitment (and application of viscous stress) is proportional to the strain. As  $\alpha$  increases above 1, low strain recruitment and corresponding viscous stress is reduced.  $K$  assigns a conventional viscosity value, which is adjusted by  $n$ , in order to account for the shear thinning. The resulting equation describes the gradual recruitment of fibers throughout extension and the strain-rate dependency of viscosity:

$$\sigma(\eta) = \left( \frac{\varepsilon}{\varepsilon_{heel}} \right)^\alpha \eta \dot{\varepsilon} = \left( \frac{\varepsilon}{\varepsilon_{heel}} \right)^\alpha K \dot{\varepsilon}^{n+1} \quad (15)$$

The full model's required inputs are summarized in Table 2, which includes values known from literature (a), structural values estimated from microscopy (b), and parameters which were estimated by phenomenological fitting (c). Currently progressing studies are employing stress relaxation, loading-unloading hysteresis, and microstructural observations during deformation in order deter-

**Table 2**

Parameters used in the viscoelastic model.

Model parameters	Values
Modulus of collagen fibril ( $E$ )	1 GPa <sup>a</sup>
Thickness of collagen fibril ( $H$ )	0.13 $\mu\text{m}^b$
Radius of curvature of collagen fibril ( $r_c$ )	7 $\mu\text{m}^b$
Degree of curvature of collagen fibril ( $\omega_0$ )	70 <sup>-b</sup>
Average misorientation from longitudinal axis ( $\gamma$ )	70 <sup>-b</sup>
Maximum fiber stiffness ( $E_{max}$ )	10 MPa <sup>c</sup>
Fiber recruitment parameter ( $\alpha$ )	2 <sup>c</sup>
Viscosity coefficient ( $K$ )	25 Pa·s <sup>c</sup>
Viscosity parameter ( $n$ )	-0.6 <sup>c</sup>

mine real viscosity values; from these studies a physically based relationship between  $\alpha$ ,  $K$ , and  $n$ , and the value of  $E_{max}$  will be established.

In order to illustrate the contributions of various parameters, the supplemental material shows multiple plots; in each case, one input is varied and the result on the mechanical response is plotted. In some cases varying certain parameters have similar effects; for example, increasing the degree of waviness and misorientation from the tensile axis both result in an extended toe region of the curve, and it is possible that similar curves can be represented with different parameters. Another example is that set  $\delta$  ratios (fiber thickness to radius of curvature) have identical responses. However, both parameters have physical significance and thus are included individually in the constitutive equation.

The four mechanisms of deformation—elastic straightening, stretching, reorientation, and sliding are accounted for in the calculated response of the skin shown in Fig. 7. The quality of fit for the various curves is quantified by calculating the average normalized root-mean-square error (*NRMSE*) for the various orientations and

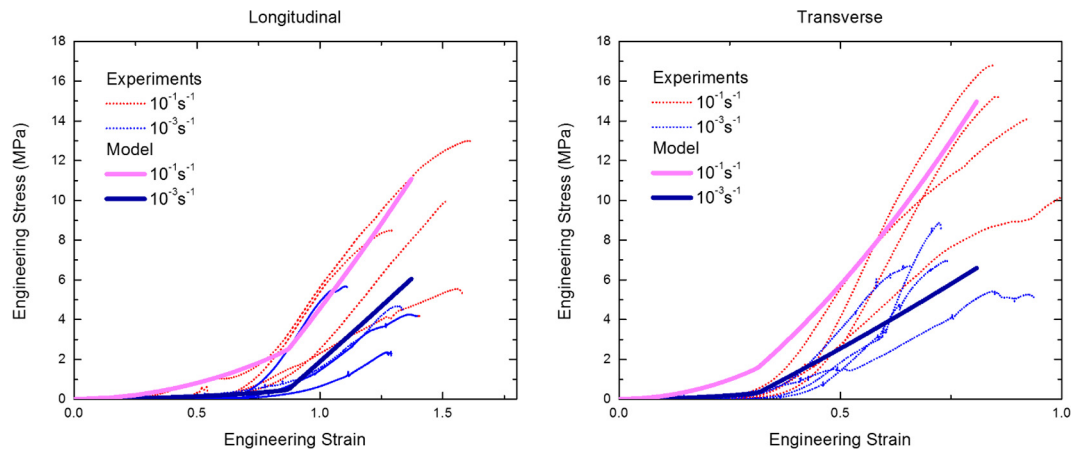


**Fig. 7.** The model as applied to test results. Tensile engineering stress-engineering strain plots made using the constitutive model are shown by the solid lines, while physical tests are shown by the dotted lines. Experimental results on rabbit skin along two orientations: longitudinal (perpendicular to Langer lines) and transverse (parallel to Langer lines) [6]. Note considerable variability among experimental results, a characteristic of skin. The model is shown to match the experimental results reasonably well, and intrinsically all values are based on the physical processes that are occurring in the skin.

strain rates. In each case, the *NRMSE* values (longitudinal  $\dot{\epsilon} = 10^{-1} : 13\%$ ,  $\dot{\epsilon} = 10^{-3} : 13\%$ ; transverse  $\dot{\epsilon} = 10^{-1} : 12\%$ ,  $\dot{\epsilon} = 10^{-3} : 12\%$ ) indicate a reasonable fit, and it is shown that the model accurately describes the response of transverse and longitudinal skin. Thus, the principal features of deforming skin are captured by the constitutive equation proposed, and are directly related its microstructure and mechanical response.

#### 4. Conclusions

This investigation connects the mechanical response of rabbit skin in uniaxial extension to the changes in the structure by providing a new constitutive equation that captures the most important processes. The following principal results are obtained:

- The dermis of the rabbit is composed of sheets or lamellae which are assemblages of curved parallel collagen fibers. In these assemblages, each layer is comprised of curved fibers with a preferential direction, different layers having different orientations. It is estimated that 250 sheets with different orientations comprise the dermis of rabbit. The fibers are, in turn, composed of fibrils.
- In tension, the collagen in these sheets straightens and aligns with the tensile direction. This requires considerable interfiber shear and sliding, and generates viscous stress as alignment leads to high stress and strain values. The combined elastic and viscous effects lead to the unique tensile response of skin, as well as its strength, versatility, and tear resistance.
- The presence of some extremely wavy fibrils is responsible for the large amounts of strain that the skin can undergo before straightening. As the less curved fibrils straighten and align, the more curved remain non-aligned. As stretching continues, the previously straight fibrils break and misalign, transferring the load to the straightening curvier fibrils. The variance between fibrils results in a large heel region as certain fibers enter their linear region, and a large failure region due to the successive breaking of the most highly stressed fibrils.
- Processes that occur in the skin during tension are represented in a constitutive equation in which the waviness is modeled as circular segments whose radius increases with extension. By including the most important physical processes in our calculations, namely straightening, stretching, reorientation and sliding (through viscosity), the stress-strain response is successfully modeled.

- Our mechanical results are limited to uniaxial testing, in which most fibers reorient parallel to the loading direction. A future possibility is to apply the model to biaxial tension; this would reduce the tensile alignment, and result in a response dominated by the straightening and sliding of collagen, but with limited reorientation.
- Understanding of the layered structure which leads to the anisotropic response, large extensibility, or tear resistance of skin has the potential to affect the development of new hyperplastic materials and synthetic skin. Biodegradable skin-like scaffolds are crucial for the improvement of integration and quality of healing; the large influence that material properties such as substrate stiffness can have on tissue growth is being increasingly recognized. By more precisely understanding the wavy structure and how it determines the stiffness of skin, biological elements of healing are likely to perform their functions more effectively, while the potential discomfort of having an inextensible or stiff synthetic skin attached to the body may be avoided.

#### 5. Disclosure

None.

#### Acknowledgements

This work was funded by the Multi-University Research Initiative grant no. AFOSR-FA9550-15-1-0009 from the Air Force Office of Scientific Research to the University of California Riverside, specifically through subcontracts to the University of California, San Diego and the University of California, Berkeley. We acknowledge the use of the UCSD Cryo-Electron Microscopy Facility which is supported by NIH grants to Dr. Timothy S. Baker and a gift from the Agouron Institute to UCSD. We gratefully acknowledge Da Le Ranch for assisting our work by fulfilling our unique order requests. Mentorship in TEM preparation and usage by Mason Mackey and Dr. Maria Isabel Lopez were invaluable, and discussions with Prof. Robert O. Ritchie and Andrei Pissarenko were key to the development of our ideas.

#### Appendix A. Supplementary data

Supplementary data associated with this article can be found, in the online version, at <http://dx.doi.org/10.1016/j.actbio.2017.02.011>.

## References

- [1] G. Dupuytren, C.F. Gräfe, M. Kalisch, Dupuytren Theoretisch-Praktische Vorlesungen Über Die Verletzungen Durch Kriegswaffen, Veit, Berlin, Germany, 1836.
- [2] K. Langer, On the anatomy and physiology of the skin. I. The cleavability of the cutis. (Translated from Langer, K. (1861). Zur Anatomie und Physiologie der Haut. I. Über die Spaltbarkeit der Cutis. Sitzungsbericht der Mathematisch-naturwissenschaftlichen Classe der Kaiserlichen Academie der Wissenschaften, Br. J. Plast. Surg. 31 (1978) 3–8.
- [3] D.R. Veronda, R.A. Westmann, Mechanical characterization of skin-finite deformations, *J. Biomech.* 3 (1970) 111–122.
- [4] G. Schwinger, K. Zanger, H. Greven, Structural and mechanical aspects of the skin of *Bufo marinus* (Anura, Amphibia), *Tissue Cell* 33 (2001) 541–547.
- [5] R.E. Shadwick, A.P. Russell, R.F. Lauff, The structure and mechanical design of rhinoceros dermal armor, *Philos. Trans. R. Soc. London, Ser. B* 337 (1992) 419–428.
- [6] W. Yang, V.R. Sherman, B. Gludovatz, E. Schaible, P. Stewart, R.O. Ritchie, M.A. Meyers, On the tear resistance of skin, *Nat. Commun.* 6 (2015).
- [7] I.V. Yannas, J.F. Burke, Design of an artificial skin. 1. Basic design principles, *J. Biomed. Mater. Res.* 14 (1980) 65–81.
- [8] J.F. Burke, I.V. Yannas, W.C. Quinby, C.C. Bondoc, W.K. Jung, Successful use of a physiologically acceptable artificial skin in the treatment of extensive burn injury, *Ann. Surg.* 194 (1981) 413–428.
- [9] B.D. Ratner, *Biomaterials Science: An Introduction to Materials in Medicine*, 3rd ed., Elsevier Academic Press, Amsterdam, Netherlands, 2013.
- [10] B.C.K. Tee, C. Wang, R. Allen, Z.N. Bao, An electrically and mechanically self-healing composite with pressure- and flexion-sensitive properties for electronic skin applications, *Nat. Nanotechnol.* 7 (2012) 825–832.
- [11] Y. Gao, A.M. Waas, J.A. Faulkner, T.Y. Kostrominova, A.S. Wineman, Micromechanical modeling of the epimysium of the skeletal muscles, *J. Biomech.* 41 (2008) 1–10.
- [12] Y. Lanir, Y.C. Fung, Two-dimensional mechanical properties of rabbit skin. II. Experimental results, *J. Biomech.* 7 (1974) 171–182.
- [13] C.J. Willmott, On the validation of models, *Phys. Geogr.* 2 (1981) 184–194.
- [14] G.D. Weinstein, R.J. Boucek, Collagen and elastin of human dermis, *J. Invest. Dermatol.* 35 (1960) 227–229.
- [15] K.H. Sizeland, R.L. Edmonds, M.M. Basil-Jones, N. Kirby, A. Hawley, S. Mudie, R. G. Haverkamp, Changes to Collagen Structure during Leather Processing, *J. Agric. Food Chem.* 63 (2015) 2499–2505.
- [16] I.C. Smith, I.-The structure of the skin and dermal scales in the tail of *acipenser ruthenus* L, *Trans. R. Soc. Edinburgh* 63 (1956) 1–14.
- [17] V.R. Sherman, W. Yang, M.A. Meyers, The materials science of collagen, *J. Mech. Behav. Biomed. Mater.* 52 (2015) 22–50.
- [18] J. Diamant, R.G.C. Arridge, E. Baer, M. Litt, A. Keller, Collagen – ultrastructure and its relation to mechanical properties as a function of aging, *Proc. R. Soc. London, Ser. B* 180 (1972) 293–315.
- [19] D.E. Beskos, J.T. Jenkins, Mechanical model for mammalian tendon, *J. Appl. Mech.* 42 (1975) 755–758.
- [20] A.D. Freed, T.C. Doebling, Elastic model for crimped collagen fibrils, *J. Biomech. Eng.* 127 (2005) 587–593.
- [21] M. Comninou, I.V. Yannas, Dependence of stress-strain nonlinearity of connective tissues on geometry of collagen-fibers, *J. Biomech.* 9 (1976) 427–433.
- [22] Y. Lanir, Structure-strength relations in mammalian tendon, *Biophys. J.* 24 (1978) 541–554.
- [23] F.P. Beer, E.R. Johnston, J.T. DeWolf, D.F. Mazurek, *Mechanics of Materials*, 5th ed., McGraw-Hill Higher Education, Boston, Massachusetts, 2009.
- [24] T. Young, *A Course of Lectures on Natural Philosophy and the Mechanical Arts*, Printed for Joseph Johnson by William Savage, London, United Kingdom, 1807.
- [25] M.T. Shaw, W.J. MacKnight, *Introduction to Polymer Viscoelasticity*, 3rd ed., Wiley, Hoboken, New Jersey, 2005.
- [26] M.A. Meyers, K.K. Chawla, *Mechanical Behavior of Materials*, Prentice Hall, Upper Saddle River, New Jersey, 1999.
- [27] J.B. Finlay, Thixotropy in human skin, *J. Biomech.* 11 (1978) 333–342.